Heliyon 9 (2023) e20380

Contents lists available at ScienceDirect

Heliyon

journal homepage: www.cell.com/heliyon

Numerical study of bacteria removal from microalgae solution using an asymmetric contraction-expansion microfluidic device: A parametric analysis approach

Ali Karimi [a], Mehdi Sattari-Najafabadi [b,*]

[a] Department of Chemical and Petroleum Engineering, Sharif University of Technology, Tehran, 14588-89694, Iran
[b] Department of Chemical Engineering, Isfahan University of Technology, Isfahan 8415683111, Iran

ARTICLE INFO

Keywords:
Inertial microfluidics
Microalgae
Bacteria removal
Numerical simulation

ABSTRACT

Microalgae have been remarkably taken into account due to their wide applications in the bio-pharmaceutical, nutraceutical and bio-energy fields. However, contamination of microalgae with bacteria still appears to be a concern, adversely impacting products' quality and process efficiency. Microalgae decontamination with conventional techniques is usually expensive and time-consuming. Moreover, damage to microalgae cells is highly possible. Asymmetric contraction-expansion microchannels (Asym-CEMCs) are promising passive microfluidic devices that can overcome conventional techniques' drawbacks with their standing-out features. However, the flexibility of Asym-CEMCs performance arising from their various tunable geometrical parameters results in the fact that their performance for separating a target particle cannot be predicted without an investigation. In this work, for the first time, Asym-CEMCs were numerically studied for the removal of a very conventional bacteria, *B. subtilis* (1 μm), from one of the most popular microalgae, *C. vulgaris* (5.7 μm). The influences of the microchannel aspect ratio, length and width ratios of the expansion-to-contraction zones, and the total flow rate on the separation resolution and focusing width of the particles were investigated by a 3D numerical model. The aspect ratio had the strongest influence on the Asym-CEMC performance, however, the length ratio had no considerable effect on the results. A decrease in the aspect ratio augmented the shear-induced lift force and Dean drag force, leading to a significant separation resolution improvement. Microalgae decontamination was also enhanced by an increase in the total flow rate and expansion-to-contraction width ratio. Finally, a locally optimized Asym-CEMC with an aspect ratio of one and expansion-to-contraction width and length ratios of 4.7 and 2.07, respectively, was proposed, leading to complete microalgae decontamination with a high normalized separation resolution of 0.6. In a word, Asym-CEMCs with tailored dimensions are promising for successfully decontaminating microalgae from bacteria.

1. Introduction

Microalgae are microscopic unicellular algae existing in marine systems and even freshwater and have been used in many applications such as biofuel production [1], wastewater treatment [2], health products [3], formulation of foods [4] and fertilizers [5].

* Corresponding author.
E-mail address: m.sattari@iut.ac.ir (M. Sattari-Najafabadi).

https://doi.org/10.1016/j.heliyon.2023.e20380
Received 21 May 2023; Received in revised form 11 September 2023; Accepted 20 September 2023
Available online 21 September 2023

Microalgae represent an enormous biodiversity, however, *C. vulgaris* microalga has been taken into notable consideration due to its wide range of applications [6]. The rigid cell wall of *C. vulgaris* remarkably protects it from harsh environments. Besides, its growth rate can simply be controlled by regulating different growth factors. The mentioned facts have made *C. vulgaris* microalga an ideal candidate to be used in a wide range of processes [6].

One of the main issues in using microalgae for different applications is bacteria contamination. This may happen during cultivation and collection processes mostly in open and semi-open microalgae cultivation methods such as raceway ponds [7]. Bacteria contamination negatively impacts the quality and production efficiency of final microalgae-based products. Among different bacteria, *B. subtilis* is a conventional source of contamination [8] that can be found in numerous sources such as soil.

Some of the most conventional purification techniques for removing bacteria from microalgae are centrifugation [9], micropipetting [10] and fluorescence activated cell sorting (FACS) [11]. The conventional methods have some drawbacks such as high cost, cell damage and time-consuming laboratory procedures in some cases [8]. To deal with the disadvantages of conventional techniques, microfluidics has been used as an emerging new technology for separation and purification processes from molecular [12–14] to microparticle scale [15–17].

Microfluidic particle separation techniques are categorized into active and passive methods [16]. In active microfluidic techniques, particles are separated by utilizing an external force that is relevant to the intrinsic properties of particles, e.g., electrical, optical and acoustic properties. Magnetophoresis [18], dielectrophoresis [19], acoustophoresis [20], and optical-force based [21] are among the main active microfluidic methods used for particle separation. On the other hand, passive techniques merely take advantage of the physical properties of particles, e.g., size, shape and density. This makes passive techniques simpler to employ for particle separation, as compared to the active methods. Passive techniques include pinch flow fractionation (PFF) [22], deterministic lateral displacement (DLD) [23] and inertial [24] techniques.

Among different passive techniques, inertial-based microfluidic devices are often preferred due to their simplicity, low cost and high throughput. Particles in inertial-based systems are separated based on the distinct focusing behavior of particles resulting from competition between the main forces, which are drag and lift forces. A wide range of microstructures have been used in inertial microfluidic devices including straight, spiral, contraction-expansion and serpentine microchannels [25]. Contraction-expansion microchannels (CEMCs) have been widely taken into consideration due to their flexible geometrical parameters, resulting in versatile functions for various purposes.

CEMCs can be mainly categorized into symmetric and asymmetric patterns based on the symmetry of the cavities. In a symmetric CEMC (Sym-CEMC), the focusing positions of the particles are also symmetric. However, in an asymmetric CEMC (Asym-CEMC), the velocity field is not symmetric, leading to different states of particle trajectories that can be adjusted by tuning the geometrical parameters of Asym-CEMCs. Due to this, there is a greater variety of structures, i.e., a more flexible performance, of Asym-CEMCs compared to that of Sym-CEMCs.

Asym-CEMCs were first used by Lee et al. [15] to focus human red blood cells. They then utilized the same geometric concept for blood plasma separation, resulting in a separation yield of 62.2% [26]. They further used Asym-CEMCs for label-free isolation of MCF-7 cancer cells from whole blood [27]. A cancer cell recovery rate of 99.1% could be achieved by adjusting the total flow rate [27]. Shin et al. [28] employed an Asym-CEMC to separate MCF-7 cancer cells from U937 lymphoma cells with an average size of 28.13 and 13.29 μm, respectively. A target cell recovery rate of 96.7% could be attained. Kim et al. [29] employed an Asym-CEMC to separate *C. vulgaris* microalga with an average diameter of 5.7 μm from *H.pulvialis* microalga having an average diameter of 24.8 μm. The widths of the contraction and expansion units of the employed microchannel were 100 and 450 μm, respectively, while the whole microchannel had a height of 80 μm. They successfully achieved a purity of 97.9% for *C. vulgaris* and 94.9% for *H.pulvialis* microalga at the device outlet. Zhu et al. [30] studied the focusing patterns of polystyrene particles in an Asym-CEMC. The particle sizes of 10, 15 and 20 μm were used to simulate human blood cells and cancer cells. The 15 and 20 μm particles could be ideally focused by adjusting the expansion region dimensions and *Reynolds* number, however, the particles of 10 μm were focused in a wide band. Recently, Wang et al. [17] proposed a 2D numerical model to study the trajectories of the 4.8 μm particles in an Asym-CEMC with triangular cavities. The microchannel feed was polyethylene oxide solutions with different concentrations to provide viscoelastic fluid behavior. They reported that the lateral migration rate of the particles was proportional to the total flow rate and inversely proportional to the polyethylene oxide concentration.

There is still a lively interest in studying Asym-CEMCs to understand their performance in focusing different target particles [17, 29–33]. Flexible performance of Asym-CEMCs due to several tunable geometrical parameters results in the fact that their performance for a specific application cannot be predicted without an investigation. In other words, for each application of an Asym-CEMC, it is essential to ensure particles of different sizes can be stably focused in a balanced position. To address this issue considering the importance of the microalgae decontamination, this work studies separation of a microalga from bacteria within Asym-CEMCs for the first time by employing a 3D numerical model. *C. vulgaris* and *B. subtilis* were selected as the model microalga and bacteria, respectively, concerning what was mentioned in the first part of this section. The size of *B. subtilis* is ~1 μm [8,34] which is at the limit of the submicron range, thus, focusing them in a narrow band through a passive inertial microfluidic device can be challenging. This can augment the necessity of the present study.

To find the geometrical parameters of an Asym-CEMC effectively influencing the focusing behavior of the mentioned particles, a comprehensive analysis was done by implementing the design of experiment (DOE) approach. The contraction-to-expansion length and width ratios and channel aspect ratio were investigated as the geometrical parameters. The total flow rate was also studied as a key operating parameter. To track the particles along the Asym-CEMC and analyze their focusing pattern, a Lagrangian particle tracing coupled with externally imported lift force data was developed and utilized. Finally, a locally optimized Asym-CEMC for removing bacteria from microalgae was proposed.

2. Physics and governing equations

The main forces exerted on the particles passing through an inertial microchannel are the viscous drag force and inertial lift force which are presented schematically in Fig. 1 as F_D and F_L, respectively. The viscous drag force affects particles in the whole microchannel, while, particles are influenced by the inertial lift force mainly as they pass through a contraction region.

The main feature of an Asym-CEMC is the formation of two counter-rotating vortices stemming from the sudden change of cross-section. These vortices result in a secondary flow, known as Dean flow, in the cross-section of the microchannel, as illustrated in Fig. 1. The Dean flow leads to the Dean drag force, aiding the particles focusing in the microchannel and improves the efficiency of the inertial-based microfluidic particle separation [35]. The Dean flow magnitude is affected directly by the *Reynolds* number and reversely by the channel (or streamline) curvature [36,37].

In this work, the Oseen's correction to the Stocks drag equation, presented as Eq. (1), was used to determine the viscous drag force. Oseen [38] made a modification to the Stocks drag equation to partially include the convective acceleration of spherical particles in a viscous, incompressible and laminar fluid flow.

$$F_D = 6\pi\mu a u\left(1+\frac{3}{8}\mathrm{Re}_p\right) \tag{1}$$

where μ, a, u and Re_p are the fluid viscosity, radius of particles, fluid velocity and particle's *Reynolds* number, respectively. Re_p is defined as $\mathrm{Re}_p = \rho u' a/\mu$, where u' is the relative velocity of the particle to the fluid and ρ is the fluid density.

The inertial lift force (F_L) acting on a spherical particle was calculated by Eq. (2) [39].

$$F_L = C_L\left(\rho a^4 G\right) = C_L\left(\frac{\rho a^4 U_f}{L}\right) \tag{2}$$

where C_L and G are the lift coefficient and local shear rate, respectively. The value of G can be approximately expressed as U_f/L where U_f and L are the average fluid velocity and characteristic length of the microchannel, respectively. L can be either the height or width of the microchannel based on the direction of the lift force being determined.

Pressure gradient force (F_{PG}) and virtual mass force (F_{VM}) are other forces being exerted on the particles and were determined by Eqs. (3) and (4), respectively. F_{PG} appears when there is a pressure difference across the particle surface. F_{VM} is the inertia added to a system since an accelerating or decelerating body must move a particular volume of encompassing fluid as it moves through it.

$$F_{PG} = \frac{\rho_p}{\rho}\left(\overrightarrow{u_p}\nabla\overrightarrow{u}\right) \tag{3}$$

$$F_{VG} = \frac{1}{2}\frac{\rho}{\rho_p}\frac{d\left(\overrightarrow{u}-\overrightarrow{u_p}\right)}{dt} \tag{4}$$

where ρ_p, $\overrightarrow{u_P}$, and $\overrightarrow{u}$ are particle density, particle velocity vector, and fluid velocity vector, respectively. The Navier-Stocks equations (Eq. 5) and the continuity equation (Eq. 6) were solved to determine the velocity field for an incompressible Newtonian fluid flow.

$$\rho\frac{\partial\overrightarrow{u}}{\partial t}+\rho(\overrightarrow{u}.\nabla)\overrightarrow{u} = -\nabla P+\mu\nabla^2\overrightarrow{u} \tag{5}$$

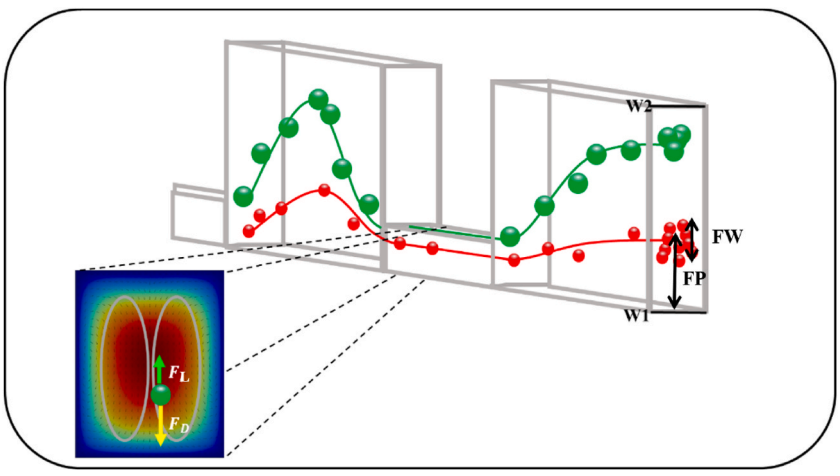

Fig. 1. The schematic of the main forces exerting on the particles passing an Asym-CEMC. W1 and W2 are the inner and outer walls of the Asym-CEMC, respectively.

$$\nabla . \vec{u} = 0 \tag{6}$$

Newton's second law (Eq. (7)) was also solved for each particle by considering the aforementioned forces exerted on the particles. It should be mentioned that Magnus force (rotation-induced lift force) and Saffman force (slip-shear induced lift force) are other hydrodynamic forces that exist in the microchannel, however, they can be ignored as they are insignificant compared to the above-mentioned forces [24].

$$m_p \frac{d\vec{u_p}}{dt} = F_D + F_L + F_{PG} + F_{VM} \tag{7}$$

where m_p is the particle mass. To predict the trajectory of particles, Lagrangian particle tracing was considered and Eq. (7) was solved. The inertial force data obtained from previously-developed machine learning-assisted method were coupled with the Lagrangian particle tracing to predict the focusing behavior of the particles in the Asym-CEMC.

The direct numerical simulation (DNS) method has been used by several scholars to estimate C_L in Eq. (2) [40]. For this purpose, the DNS method solves the Navier-Stocks equations (Eq. 5) coupled with the particle motions equation (Eq. 7). The DNS method is often time-consuming, however, they are more accurate than other methods, such as asymptotic analysis which was found to have less accuracy for lift coefficient determination in deep CEMCs [41]. In this work, to reduce the time required for the C_L estimation, the machine-learning-based method developed by Su et al. [42] was used. They built a comprehensive library for the lift coefficient exerting on a particle at different conditions and implemented a machine learning algorithm for ultra-fast prediction of the lift coefficient.

3. Methodology

The Asym-CEMC studied in this work is shown in Fig. 2. It was straight, having a quadrilateral cross-section and consisting of various contraction units followed by expansion units. The aspect ratio (AR), length ratio (LR) and width ratio (WR) were the investigated geometrical parameters. The AR in this study was defined as WC/H where WC was the width of the contraction channel and H was the microchannel height, perpendicular to the paper in Fig. 2. The WR was defined as the ratio of the expansion unit width (WE) to the WC ($WR = WE/WC$). The LR was the ratio of the contraction unit length (LC) to the expansion unit length (LE) ($LR = LC/LE$). The height of all investigated Asym-CEMCs in this study (H) was set to 14 μm. Moreover, a constant LC of 400 μm was considered for all cases. The total length of the Asym-CEMC varied by changing the LR in this study, however, it does not affect the separation process in the optimized Asym-CEMC. This will be discussed in section 4.6. Total flow rate (TFR) was also considered as an operational parameter affecting the separation of particles. Table 1 summarizes the parameters and levels which were studied in this work. It should be noted that the effect of the expansion zone aspect ratio was also examined in this work since $WR = AR_{\text{exp ansion}}/AR_{contraction}$.

Two main response parameters, namely the separation resolution and focusing width of the 1 μm particles (FW1), were considered for the analysis. The resolution was defined as the distance between the focusing positions (FPs) of the particles with two different sizes at the microchannel outlet. The FP of the particles with a specific size was the average position of those particles at the microchannel outlet with respect to the inner wall of the microchannel (W1 in Fig. 1). The FW1 was defined as twice the standard deviation of the FP of the 1 μm particles at the microchannel outlet. All response values were normalized by dividing them by the WE value and then were reported in this work. Average Dean velocity (ADV) was also used as a side parameter representing the strength of the Dean flow formed in the CEMCs.

A face-centered central composite design (FC-CCD) with a total number of 31 tests (16 factorial points, 7 center points and 8 axial points) was utilized to investigate the effect of the above-mentioned parameters on the separation efficiency of the Asym-CEMC. A one-way analysis of variation (ANOVA) test was carried out at a confidence level of 95% for statistical significance and active effects determination. For factor screening, the effects with a p-value less than 0.05 were considered to be significant. The DOE and whole analysis of the results were performed using the *Minitab* software v.19.0. The complete DOE matrix is summarized in Table S1 as the supplementary materials.

The *COMSOL Multiphysics v6.0* software was employed to numerically carry out the designed tests. Inlet-1 and inlet-2 (see Fig. 2) were allocated to the sample (the particle mixture) and sheath flows, respectively. A total number of 100 particles were released from inlet-1 in each simulation. The sample to sheathe flow rate ratio was set to 1:9. Water was added as the main fluid, flowing in the microchannel. Normal inflow velocities and zero-static pressure were set as the inlet and outflow boundary conditions, respectively.

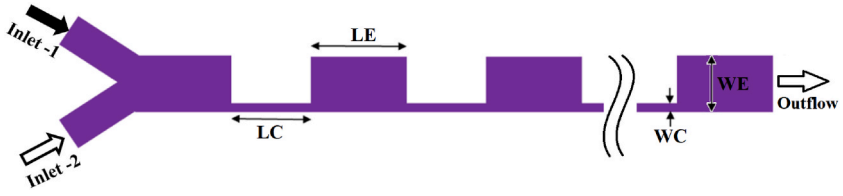

Fig. 2. The dimensions of the Asym-CEMC studied in this work.

Table 1
The parameters and corresponding levels studied in this work.

Parameter	Levels		
	−1	0	+1
Aspect Ratio, AR	1	2	3
Width Ratio, WR	3	4.5	6
Length Ratio, LR	1	2	3
Total Flow Rate, TFR (μL/min)	10	20	30

Regarding what was mentioned in section 1, to represent *C. vulgaris* microalga and *B. subtilis* bacteria in this study, the 5.7 [29] and 1 μm [8] particles, respectively, were defined in the *COMSOL Multiphysics* software. The entire geometries utilized in this study were meshed by the structured mapped mesh, as illustrated in Fig. 3.

4. Results and discussion

4.1. Validation and mesh independency

To validate the numerical model, the obtained data from the model were compared with the experimental data reported by Kim et al. [29]. They used an Asym-CEMC for the separation of two types of microalgae with the diameters of 5.7 and 24.8 μm as the *Reynolds* number ranged from 1 to 15. The values of the WC, LC, H, WR and LR in their work were 100 μm, 1200 μm, 80 μm, 4.5 and 1.7, respectively. Fig. 4A graphically compares the particle trajectories observed experimentally by Kim et al. [29] with those of the numerical model for the 5.7 μm particles, showing a good agreement between the model predictions and the experimental results. The normalized FPs and FWs of the particles under various *Reynolds* numbers are also compared in Fig. 4B. For the 24.8 μm particles, the overall variation trend obtained from the model agreed with that of the experimental data. However, the prediction error of the FPs increased with the *Reynolds* number, leading to an average relative error of 15%. The errors are calculated by Eq. (8). For the particles of 5.7 μm, the FPs obtained from the model showed an average relative error of 12%, as compared to those observed experimentally. Besides, the FW of the 5.7 μm particles was predicted with an average error of less than 50%. It could be then concluded that the model results were in a good agreement with those experimentally reported.

$$\%\ \text{relative error} = \frac{|(\text{simulation derived value}) - (\text{experimental value})|}{(\text{experimental value})} \times 100 \tag{8}$$

Mesh independency analysis was also performed by changing the number of the mesh elements and exploring the lateral velocity profiles along the microchannel width after an expansion unit where the Dean flow intensified. The results are shown in Fig. 4C. The element size in the range investigated in Fig. 4C had an insignificant influence on the obtained results. Thus, the largest element size was chosen for further investigations in this work to reduce the computation time. This led to a total element number of 6×10^4 to 1.5×10^5 for each Asym-CEMC, depending on the dimensions of the studied microchannel.

4.2. Analysis of variance

Table 2 presents the ANOVA results for the separation resolution, FW1 and ADV. Regarding the *p*-values, two investigated factors out of four, namely the AR and TFR, had significant effects on the resolution. Moreover, the interaction effects of the AR with the WR and TFR were determined to have considerable influences on the resolution. The results suggested no significant dependence of the FW1 on the studied parameters and only the interaction effect of the AR and LR was found to be significant. The ADV was significantly affected by the LR and TFR, as well as the interaction effects of the AR with the WR, and the interaction effects of the LR with the WR and TFR. The R^2 and adjusted R^2 values for the resolution model were 76.7% and 61.7%, respectively. They were 58.3% and 21.8%,

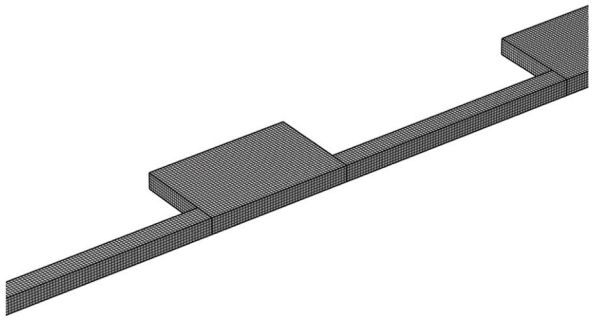

Fig. 3. The employed mesh geometry.

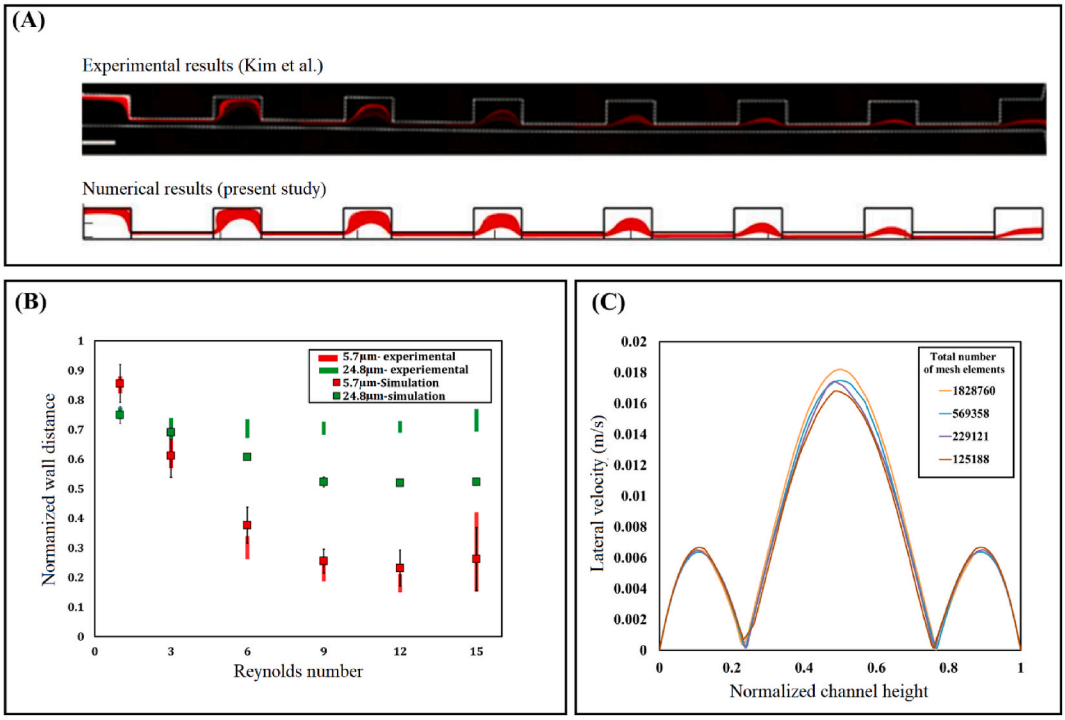

Fig. 4. Comparing the data obtained from the model with those reported by Kim et al. [26] (A) the particle trajectories of the 5.7 μm particles, (B) the normalized focusing position and focusing width values. For the numerical data, the filled cubes and the corresponding black error bars are the FP and FW, respectively. The focusing region of the particles observed experimentally by Kim et al. [26] are depicted in pale red and green bars. (C) the lateral velocity along the channel height for different mesh elements number.

Table 2
The ANOVA results for the resolution, FW1 and ADV.

	Resolution		FW1		ADV	
Source	Adjusted Mean Square	*p*-value	Adjusted Mean Square	*p*-value	Adjusted Mean Square	*p*-value
AR	0.177730	0.000****	0.003117	0.171	0.000055	0.839
LR	0.015845	0.197	0.000016	0.919	0.013669	0.005**
WR	0.003903	0.513	0.002918	0.185	0.00264	0.171
TFR	0.054695	0.024*	0.000766	0.488	0.052183	0.000****
AR^2	0.070135	0.012*	0.001971	0.313	0.000355	0.607
LR^2	0.029546	0.085	0.005331	0.079	0.000025	0.889
WR^2	0.000096	0.918	0.000326	0.649	0.000026	0.896
TFR^2	0.003741	0.522	0.002273	0.239	0.000149	0.739
AR*LR	0.005166	0.453	0.012940	0.010*	0.001067	0.376
AR*WR	0.089872	0.005**	0.000486	0.579	0.013853	0.005**
AR*TFR	0.069607	0.012*	0.000826	0.471	0.000004	0.955
LR*WR	0.000144	0.899	0.001272	0.374	0.006286	0.042*
LR*TFR	0.006062	0.417	0.003688	0.139	0.010770	0.011*
WR*TFR	0.000015	0.967	0.000031	0.889	0.001162	0.356
Lack-of fit	0.013864		0.002429		0.002061	
Pure error	0.000190		0.000000		0.000000	

$P < 0.05$ was considered to indicate a statistically significant difference.
*$P < 0.05$, **$P < 0.01$, ***$P < 0.001$, ****$P < 0.0001$.

respectively, for the FW1 model and also 83.5% and 69% for the ADV model. The results will be elaborated on through the following sections.

4.3. Effect of aspect ratio

The ANOVA results revealed that the AR was the most important parameter affecting the resolution. Fig. 5 shows the effect of the AR on the resolution at different WRs. A decrease in the AR led to a considerable enhancement of the resolution. To identify the cause of the observed trend, the cross-sectional views of the particles' distribution at the outlet of the Asym-CEMCs with different ARs are

presented in Fig. 6A. The AR significantly affected the focusing of both particle sizes. Basically, altering AR may influence two phenomena in the Asym-CEMC: 1) the shear rate gradient and 2) the Dean flow strength.

The shear rate suddenly dropped as the fluid exited a contraction region and entered an expansion zone, as illustrated in Fig. 6B. This led to a shear rate gradient in the Asym-CEMC, resulting in a change in the shear-induced lift force exerted on the particles. The shear-induced lift force is strongly proportional to the particle size (Eq. (2)), therefore, its influence on the larger particles was stronger than that on the smaller particles, pushing them toward the outer wall of the microchannel (W2 in Fig. 1). Regarding Fig. 6C, decrement of the AR remarkably augmented the shear rate gradient, i.e., the shear-induced lift force in the microchannel. Hence, a larger displacement of the 5.7 μm particles toward W2 occurred as the AR was decreased.

On the other hand, decreasing AR led to the Dean flow enhancement. As the Dean flow influences the smaller particles more intensely compared to the larger particles, decreasing the AR pushed the 1 μm particles downward the W1 of the Asym-CEMC. Two simultaneous consequences of the AR decrement on the shear-induced lift force as well as the Dean flow strength resulted in the improvement of the separation resolution.

The ANOVA analysis also suggested that the AR can affect the FW1 depending on the LR value (AR*LR p-value<0.05). Fig. 7 presents the influence of the AR on the FW1 at different LR values, revealing that the FW1 was mainly influenced by the AR while LR was set to one. The inertial focusing become significant as the blockage ratio ($\kappa = a/D_h$, where a and D_h are the particle size and microchannel hydraulic diameter, respectively) exceeds 0.07 [43]. The blockage ratio of the 1 μm particles increased by the AR decrement (the D_h decrement) and it exceeded 0.07 as the AR was reduced to one. Therefore, the inertial focusing of the 1 μm particles became significant and then, the FW1 was narrowed by the AR decrease.

4.4. Effect of width ratio

The increase of the WR generally improved the separation resolution, as shown in Fig. 5. Obviously, increasing the WR resulted in an increase in the difference between the widths of the expansion and contraction zones. Then, the fluid passing the Asym-CEMC experienced a higher pressure drop and the curvature of the fluid flow streamlines altered. This finally could result in the enhancement of the ADV and thus, the Dean flow strength. The increase of the Dean flow with the WR could augment the movement of the smaller particles toward the W1 of the microchannel and therefore, the resolution was enhanced.

As shown in Fig. 5, the improvement of the resolution with the WR was more profound in a smaller AR. This is due to the fact that the effect of the shear gradient lift force on the particle separation became stronger in a smaller AR, as discussed through the previous section. Hence, an increase of the WR in the smaller ARs could lead to a larger improvement of the ADV and then the separation resolution.

4.5. Effect of total flow rate

Fig. 8A presents the influence of the TFR on the separation resolution. The increment in the TFR led to an increase in the resolution. Fig. 8B shows the cross-sectional velocity profiles at a distance of 7 μm after an expansion unit (where the Dean flow strength was considerable) for the Asym-CEMC with AR = 1 under different flow rates. Arrows show the direction and magnitude of the generated Dean velocity in the selected cut-plane, revealing that increasing TFR augmented the ADV and then, the Dean flow strength was improved. Besides, the ANOVA results for the ADV presented in Table 2 shows that the TFR was determined the most important parameter affecting the Dean flow strength in the Asym-CEMC. Zhao et al. [35] also observed enhancement of the Dean flow strength with the TFR. The improvement of the Dean flow strength led to an augmentation in the Dean Drag force on the smaller particles pushing them toward the W1 of the microchannel. On the other side, the increase in the TFR, i.e., increase of the average flow velocity, enhanced the shear-induced lift force in the expansion zone (see Eq. (2)), resulting in a larger displacement of the 5.7 μm particles toward the W2 of the microchannel. Two mentioned simultaneous consequences led to the observed increase of the separation resolution with TFR.

The ANOVA results also suggested that the interaction of the TFR and AR had a considerable influence on the resolution. In other words, the effect of the TFR became more significant in a lower AR, as shown in Fig. 8A. This was due to the fact that the shear rate gradient was increased 3.34-fold and 2.18-fold as the TFR was increased from 10 to 30 μL/min in the Asym-CEMC with the AR of one

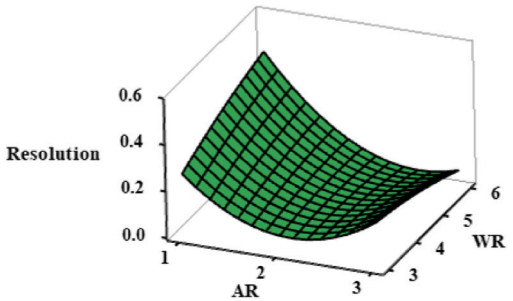

Fig. 5. The effects of the AR and WR on the separation resolution (middle point hold values are used.).

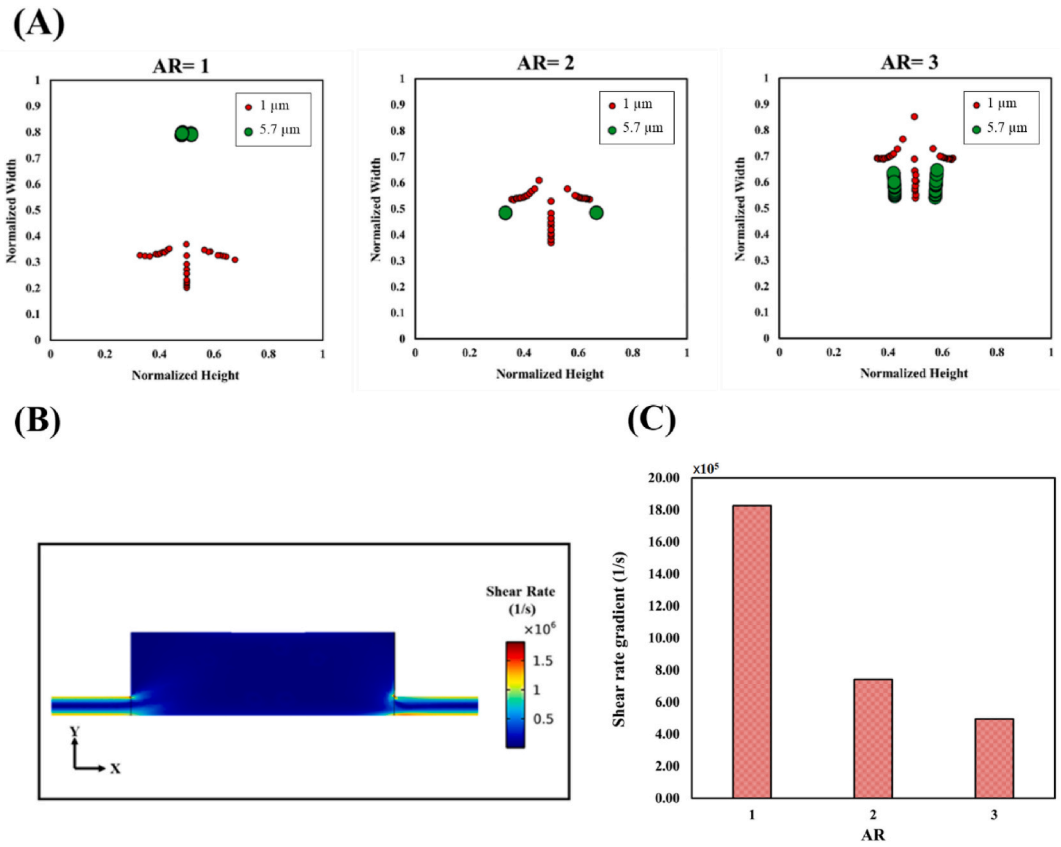

Fig. 6. (A) Cross-sectional distribution of the particles at the outlet of the Asym-CEMC with different ARs, (B) the shear rate contour in the Asym-CEMC with AR = 1, (C) comparing the shear rate gradient in the Asym-CEMCs with different ARs. The results correspond to WR = 4.5, LR = 2 and TFR = 20 μL/min.

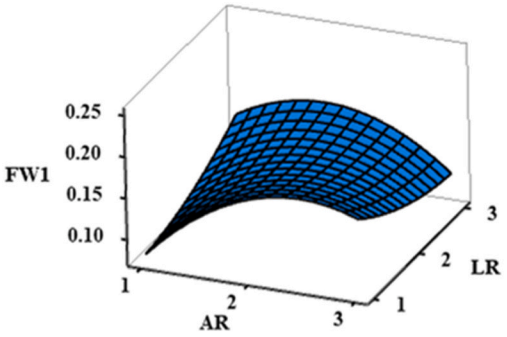

Fig. 7. The FW1 versus the AR and LR (middle point hold values are used.).

and three, respectively. Therefore, improvement of the shear-induced lift force by the TFR was more intense at a smaller AR, leading to a stronger enhancement of the resolution by the TFR in the smaller ARs.

4.6. Locally optimized design

To achieve a local optimum for the efficient separation of the bacteria (1 μm) from the microalgae (5.7 μm), a multiple response optimization was conducted aiming at maximizing and minimizing the resolution and FW1, respectively. Fig. 9 presents the result of the optimization obtained from *Minitab* software. A Asym-CEMC with AR = 1, LR = 2.07 and WR = 4.7 as the TFR was set to 30 μL/min was predicted to results in a separation resolution of 0.51 and the FW1 of 0.10 (with a composite desirability of 0.76). The final overall length of the optimized Asym-CEMC is approximately 4.1 mm. Besides, the length of the contraction channel in each unit of the

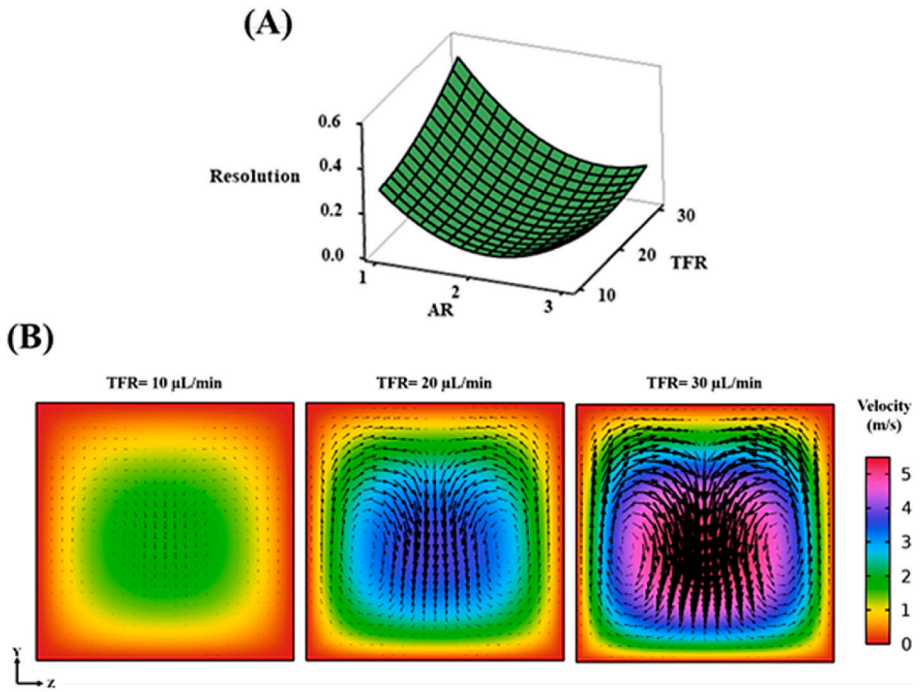

Fig. 8. (A) The influence of the TFR on the separation resolution at different ARs and (B) the cross-sectional velocity profiles for different TFRs. The arrows show the direction and magnitude of the generated secondary flows.

optimized Asym-CEMC is 400 µm. The minimum length, $L_{\min}$, required for achieving an equilibrium position for 5.7 µm particle (the target particle in this study) can be estimated by $L_{\min} = \pi\mu H^2 / (\rho U_m a^2 \overline{C_L})$ [44] where U_m is the average fluid velocity and $\overline{C_L}$ is the average lift coefficient in the contraction channel. By employing the values corresponding to the optimized Asym-CEMC, the

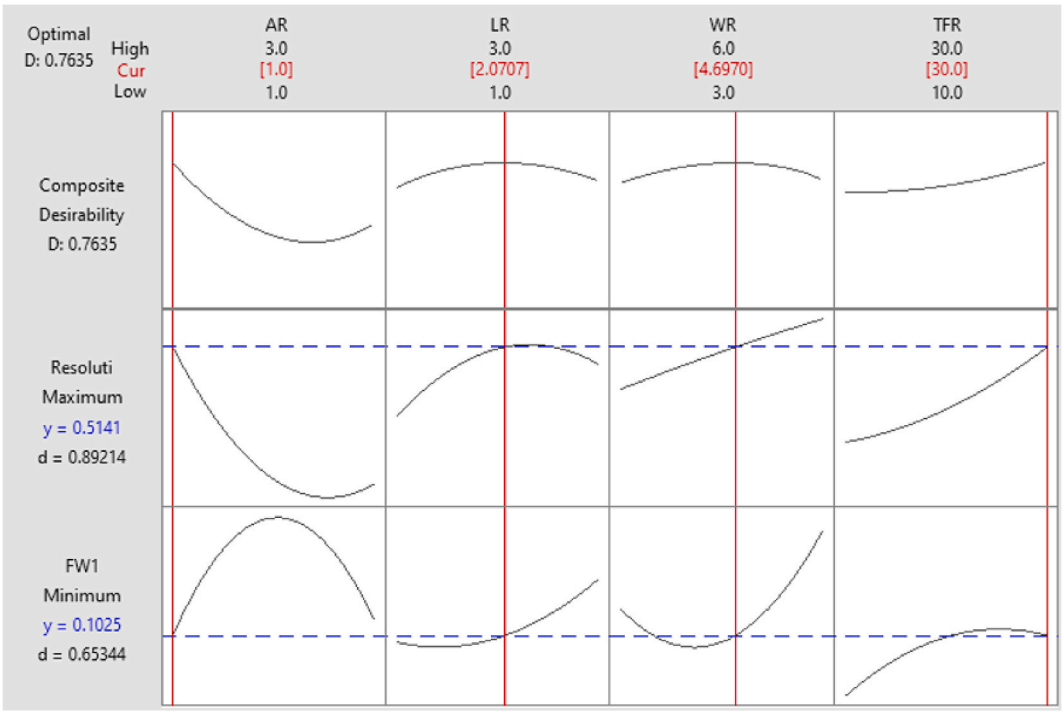

Fig. 9. The results of multi-response optimization for the resolution and FW1.

mentioned equation estimates the L_{min} to be 375 μm which is slightly shorter than that of the optimal device (400 μm).

By considering the above-mentioned optimized values for the Asym-CEMC and performing the simulation by the *COMSOL Multiphysics* software, the resulting values for the resolution and FW1 were 0.59 and 0.15, respectively. Fig. 10A and B shows the particle trajectory along the optimized Asym-CEMC and particle distribution at the end of the microchannel, respectively.

Table 3 compares the results of the present work with those reported for Asym-CEMCs in the literature. The dimensions summarized in the table correspond to the device in each work that led to the best results. The smallest particles in most of the previous studies were remarkably larger than 1 μm, however, the obtained normalized separation resolution in this study was considerably higher than those reported in some previous works. This shows that an Asym-CEMC with tailored geometrical and operating parameters has a great potential for achieving a complete separation of bacteria from microalgae and further experimental investigations are strongly recommended.

4.7. Challenges

Although the proposed optimized Asym-CEMC is capable of decontaminating microalgae from bacteria, there are some challenges that may be of interest to future works. As discussed previously in section 1, *C. vulgaris* and *B. subtilis* were investigated in this study since they are conventional microalga and contaminant, respectively. However, the inertial-based separation of particles is highly dependent on the size of each particle group. Therefore, the dimensions of an Asym-CEMC need to be tailored case by case for mixtures of microalgae and bacteria with different sizes. Moreover, the size difference has a crucial role in the separation resolution of this system. A smaller size difference of particles makes the separation more difficult, however, separation can be enhanced by modifying the device geometry [16].

Microfluidic particle separating systems often suffer from low flow rates that are far from the industrial scale. To address this challenge, the numbering-up approach can be employed. In other words, a bundle of Asym-CEMCs can be parallelized to increase the working flow rate of the microalgae decontamination process. In this regard, feed liquids have to be equally distributed at the inlets of the parallel Asym-CEMCs. Flow distributors for microfluidic systems are being developed to deal with the scale-up challenge of these devices [45–47].

Inertial microfluidic devices in lab scale are normally fabricated from polydimethylsiloxane (PDMS) which is flexible and expensive, and has low mechanical and chemical resistances. Conventional thermoplastics such as poly(methyl methacrylate), polycarbonate and polystyrene can be used to fabricate microfluidic devices for industrial purposes. In this regard, it is suggested to first fabricate a limited number of metallic molds of the microfluidic device with the desired geometry and dimensions by the micro-milling method. Then, a large number of final microfluidic devices can be fabricated using the mentioned molds and molten thermoplastics.

Finally, in industrial applications, microalgae mixtures may include large particles leading to microchannel clogging. To avoid this, it is suggested to pre-filter the feed mixture to eliminate particles larger than the target ones.

5. Conclusion

Microalgae are used in various fields including biopharmaceuticals, nutraceuticals and bio-energy. However, the related processes suffer from the contamination of microalgae solutions by bacteria. Centrifugation, micropipetting and fluorescence activated cell sorting are some of the conventional methods for microalgae decontamination. These methods are mostly expensive and time-consuming, causing considerable cell damage. Asymmetric contraction-expansion microchannels (Asym-CEMCs) are promising passive microfluidic devices that can overcome the drawbacks of the conventional methods. However, the performance of an Asym-CEMC can be highly varied by changing its various geometrical parameters. Therefore, for a desired application, it is required to examine if target particles with certain sizes can be stably focused within an Asym-CEMC. In the present study, an Asym-CEMC was numerically investigated, employing the design of experiment (DOE) approach, to separate *C. vulgaris* microalga from *B. subtilis* bacteria with the average size of 5.7 and equivalent diameter of 1 μm, respectively. The Asym-CEMC had two inlets, allocated to the microalga/bacteria solution and sheath flow. The effects of the microchannel aspect ratio, and length and width ratios of the expansion-to-contraction zones as the geometrical parameters and the total flow rate as the operating parameter on the separation resolution and focusing width of the particles were studied.

Regarding the results, the aspect ratio had the greatest influence on the separation resolution compared to that of the other studied parameters. Reducing the aspect ratio significantly enhanced the resolution due to the improved shear-induced lift force and Dean drag force. The former pushed the microalga particles toward the outer wall of the microchannel, while the latter caused a larger movement of the bacteria particles toward the inner wall. The focusing width of the bacteria at the microchannel outlet was narrowed by the aspect ratio decrease. This effect became remarkable as the contraction-to-expansion length was reduced. The increase in the width ratio had a positive effect on the Dean flow enhancement and separation resolution particularly in a smaller aspect ratio which was due to the shear gradient lift force when fluid passed through the contraction-expansion channel. An increase in the total flow rate augmented the Dean flow velocity and shear-induced lift force, leading to an enhancement in the separation resolution.

Finally, the Asym-CEMC was locally optimized to simultaneously maximize the separation resolution and minimize the particle focusing width, leading to the complete separation of bacteria from the microalgae solution. The design optimization led to an Asym-CEMC with an aspect ratio of one and an expansion-to-contraction unit length ratio of 4.7 while the total flow rate was set to 30 μL/min. The obtained results show that Asym-CEMCs have a great potential for successful microalgae decontamination and further experimental studies may be conducted to better understand an Asym-CEMC's performance for this purpose.

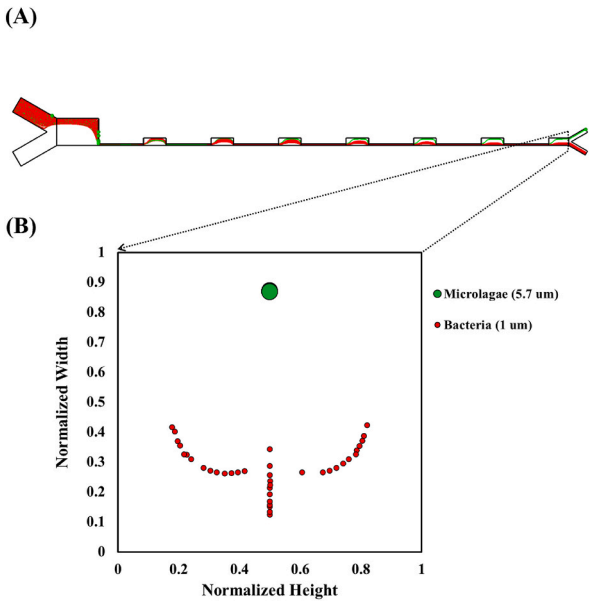

Fig. 10. (A) The particle trajectory along the optimized Asym-CEMC and (B) the particle distribution at the end of the optimized Asym-CEMC.

Table 3
Comparison of the optimized Asym-CEMC with those reported in the literature.

Particles (Size in μm)	AR	LR	WR	TFR	Separation Resolution	Reference
Polystyrene beads (4, 10)	1.0, 2.5	0.4	7.0	Re = 12.5	0.33 (AR = 1) 0.05 (AR = 2.5)	[42]
Polystyrene beads (4, 10, 15) MCF-7 and blood cells (N/A)	0.8	1.7	7.0	6.2 mL/h	0.25 (4 and 10 μm) 0.54 (4 and 15 μm) 0.36 (MCF-7 and blood cells)	[24]
MCF-7 and U937 cells (28.13, 13.29)	0.9	4.6	7.0	8.8 mL/h	0.35	[25]
Microalgae (5.7, 24.8)	1.3	1.7	4.5	7.4 mL/h	0.48	[26]
Polystyrene beads (10, 15, 20)	4.8	1.0	2.0	$Re < 10$	0.10 (10 and 20 μm)	[27]
Bacteria and microalgae (1, 5.7)	1.0	2.1	4.7	30 μL/min	0.59	Present study

Author contribution statement

Ali Karimi: Conceived and designed the analysis; Analyzed and interpreted the data; Contributed analysis tools or data; Wrote the paper.

Mehdi Sattari-Najafabadi: Analyzed and interpreted the data; Contributed analysis tools or data; Wrote the paper.

Data availability statement

Data included in article/supp. material/referenced in article.

Declaration of competing interest

The authors declare that they have no known competing financial interests or personal relationships that could have appeared to influence the work reported in this paper.

Appendix A. Supplementary data

Supplementary data to this article can be found online at https://doi.org/10.1016/j.heliyon.2023.e20380.

References

[1] K.K. Lum, J. Kim, X.G. Lei, Dual potential of microalgae as a sustainable biofuel feedstock and animal feed, J. Anim. Sci. Biotechnol. 4 (1) (2013) 53, https://doi.org/10.1186/2049-1891-4-53.

[2] N. Rashid, W.K. Park, T. Selvaratnam, Binary culture of microalgae as an integrated approach for enhanced biomass and metabolites productivity, wastewater treatment, and bioflocculation, Chemosphere 194 (2018) 67–75, https://doi.org/10.1016/j.chemosphere.2017.11.108.

[3] I. Barkia, N. Saari, S.R. Manning, Microalgae for high-value products towards human health and Nutrition, Mar. Drugs 17 (5) (2019) 304, https://doi.org/10.3390/md17050304.

[4] R. Kratzer, M. Murkovic, Food ingredients and nutraceuticals from microalgae: main product classes and biotechnological production, Foods 10 (7) (2021) 1626, https://doi.org/10.3390/foods10071626.

[5] A.K.A. Suleiman, K.S. Lourenço, C. Clark, R.L. Luz, G.H.R. da Silva, L.E.M. Vet, H. Cantarella, T.V. Fernandes, E.E. Kuramae, From toilet to agriculture: fertilization with microalgal biomass from wastewater impacts the soil and rhizosphere active microbiomes, greenhouse gas emissions and plant growth, Resour. Conserv. Recycl. 161 (2020), 104924, https://doi.org/10.1016/j.resconrec.2020.104924.

[6] C. Safi, B. Zebib, O. Merah, P.Y. Pontalier, C. Vaca-Garcia, Morphology, composition, production, processing and applications of Chlorella vulgaris: a review, Renew. Sustain. Energy Rev. 35 (2014) 265–278, https://doi.org/10.1016/j.rser.2014.04.007.

[7] A. Bani, F.G.A. Fernandez, G. D'Imporzano, K. Parati, F. Adani, Influence of photobioreactor set-up on the survival of microalgae inoculum, Bioresour. Technol. 320 (2021), 124408, https://doi.org/10.1016/j.biortech.2020.124408.

[8] D. Yuan, Q. Zhao, S. Yan, S.Y. Tang, Y. Zhang, G. Yun, N.T. Nguyen, J. Zhang, M. Li, W. Li, Sheathless separation of microalgae from bacteria using a simple straight channel based on viscoelastic microfluidics, Lab Chip 19 (17) (2019) 2811–2821, https://doi.org/10.1039/C9LC00482C.

[9] S.I. Heaney, G.H.M. Jaworski, A simple separation technique for purifying micro-algae, Br. Phycol. J. 12 (2) (1977) 171–174, https://doi.org/10.1080/00071617700650191.

[10] R.A. Andersen, Algal Culturing Techniques, Elsevier Science, 2005.

[11] M. Cellamare, A. Rolland, S. Jacquet, Flow cytometry sorting of freshwater phytoplankton, J. Appl. Phycol. 22 (1) (2010) 87–100, https://doi.org/10.1007/s10811-009-9439-4.

[12] Y. Amini, A. Hassanvand, V. Ghazanfari, M.M. Shadman, M. Heydari, Z.S. Alborzi, Optimization of liquid-liquid extraction of calcium with a serpentine microfluidic device, Int. Commun. Heat Mass Tran. 140 (2023), 106551, https://doi.org/10.1016/j.icheatmasstransfer.2022.106551.

[13] P. Abdollahi, J. Karimi-Sabet, M.A. Moosavian, Y. Amini, Microfluidic solvent extraction of calcium: modeling and optimization of the process variables, Sep. Purif. Technol. 231 (2020), 115875, https://doi.org/10.1016/j.seppur.2019.115875.

[14] S. Marsousi, J. Karimi-Sabet, M.A. Moosavian, Y. Amini, Liquid-liquid extraction of calcium using ionic liquids in spiral microfluidics, Chem. Eng. J. 356 (2019) 492–505, https://doi.org/10.1016/j.cej.2018.09.030.

[15] M.G. Lee, S. Choi, J.-K. Park, Three-dimensional hydrodynamic focusing with a single sheath flow in a single-layer microfluidic device, Lab Chip 9 (21) (2009) 3155–3160, https://doi.org/10.1039/B910712F.

[16] H. Cha, H.A. Amiri, S. Moshafi, A. Karimi, A. Nikkhah, X. Chen, H.T. Ta, N.-T. Nguyen, J. Zhang, Effects of obstacles on inertial focusing and separation in sinusoidal channels: an experimental and numerical study, Chem. Eng. Sci. 276 (2023), 118826, https://doi.org/10.1016/j.ces.2023.118826.

[17] T. Wang, D. Yuan, W. Wan, B. Zhang, Numerical study of viscoelastic microfluidic particle manipulation in a microchannel with asymmetrical expansions, Micromachines 14 (2023) 915.

[18] A. Munaz, M.J.A. Shiddiky, N.T. Nguyen, Recent advances and current challenges in magnetophoresis based micro magnetofluidics, Biomicrofluidics 12 (3) (2018), 031501, https://doi.org/10.1063/1.5035388.

[19] M. Farasat, E. Aalaei, S. Kheirati Ronizi, A. Bakhshi, S. Mirhosseini, J. Zhang, N.-T. Nguyen, N. Kashaninejad, Signal-based methods in dielectrophoresis for cell and particle separation, Biosensors 12 (7) (2022) 510.

[20] Y. Gao, M. Wu, Y. Lin, J. Xu, Acoustic microfluidic separation techniques and bioapplications: a review, Micromachines 11 (10) (2020) 921.

[21] N.-T. Huang, H.-l. Zhang, M.-T. Chung, J.H. Seo, K. Kurabayashi, Recent advancements in optofluidics-based single-cell analysis: optical on-chip cellular manipulation, treatment, and property detection, Lab Chip 14 (7) (2014) 1230–1245, https://doi.org/10.1039/C3LC51211H.

[22] A. Jain, J.D. Posner, Particle dispersion and separation resolution of pinched flow fractionation, Anal. Chem. 80 (5) (2008) 1641–1648, https://doi.org/10.1021/ac0713813.

[23] T. Salafi, Y. Zhang, Y. Zhang, A review on deterministic lateral displacement for particle separation and detection, Nano-Micro Lett. 11 (1) (2019) 77, https://doi.org/10.1007/s40820-019-0308-7.

[24] J. Zhang, S. Yan, D. Yuan, G. Alici, N.-T. Nguyen, M. Ebrahimi Warkiani, W. Li, Fundamentals and applications of inertial microfluidics: a review, Lab Chip 16 (1) (2016) 10–34, https://doi.org/10.1039/C5LC01159K.

[25] W. Tang, S. Zhu, D. Jiang, L. Zhu, J. Yang, N. Xiang, Channel innovations for inertial microfluidics, Lab Chip 20 (19) (2020) 3485–3502, https://doi.org/10.1039/D0LC00714E.

[26] M.G. Lee, S. Choi, H.-J. Kim, H.K. Lim, J.-H. Kim, N. Huh, J.-K. Park, Inertial blood plasma separation in a contraction–expansion array microchannel, Appl. Phys. Lett. 98 (25) (2011), 253702, https://doi.org/10.1063/1.3601745.

[27] M.G. Lee, J.H. Shin, C.Y. Bae, S. Choi, J.-K. Park, Label-free cancer cell separation from human whole blood using inertial microfluidics at low shear stress, Anal. Chem. 85 (13) (2013) 6213–6218, https://doi.org/10.1021/ac4006149.

[28] J.H. Shin, M.G. Lee, S. Choi, J.-K. Park, Inertia-activated cell sorting of immune-specifically labeled cells in a microfluidic device, RSC Adv. 4 (74) (2014) 39140–39144, https://doi.org/10.1039/C4RA06296E.

[29] G.-Y. Kim, J. Son, J.-I. Han, J.-K. Park, Inertial microfluidics-based separation of microalgae using a contraction–expansion array microchannel, Micromachines 12 (1) (2021) 97.

[30] G. Zhu, Z. Zhang, X. Shi, W. Tan, Experimental study on inertial focusing pattern in asymmetric contraction–expansion array microchannel, Microfluid. Nanofluidics 26 (1) (2022) 5, https://doi.org/10.1007/s10404-021-02510-2.

[31] R. Nasiri, A. Shamloo, J. Akbari, P. Tebon, M.R. Dokmeci, S. Ahadian, Design and simulation of an integrated centrifugal microfluidic device for CTCs separation and cell lysis, Micromachines 11 (2020) 699.

[32] X. Shi, W. Tan, Y. Lu, J. Ying, G. Zhu, A Virtual Boundary Method in Asymmetric Contraction-Expansion Array Channel for Focusing Pattern Prediction (2022). Available at: SSRN: https://ssrn.com/abstract=4255419.

[33] Z. Wang, T. Zhen, F. Wu, S. Mo, L. Jia, Y. Chen, Enhanced particle focusing and sorting by multiple sheath stream in contraction–expansion microchannel, Microfluid. Nanofluidics 27 (2) (2023) 16, https://doi.org/10.1007/s10404-022-02620-5.

[34] A. Katz, A. Alimova, X. Min, E. Rudolph, M.K. Shah, H.E. Savage, R.B. Rosen, S.A. McCormick, R.R. Alfano, Bacteria size determination by elastic light scattering, IEEE J. Sel. Top. Quant. Electron. 9 (2) (2003) 277–287, https://doi.org/10.1109/JSTQE.2003.811284.

[35] Q. Zhao, D. Yuan, J. Zhang, W. Li, A review of secondary flow in inertial microfluidics, Micromachines 11 (5) (2020) 461.

[36] W.R. Dean, XVI. Note on the motion of fluid in a curved pipe, London, Edinburgh Dublin Phil. Mag. J. Sci. 4 (20) (1927) 208–223, https://doi.org/10.1080/14786440708564324.

[37] S.A. Berger, A.L. Talbot, L.S. Yao, Flow in curved pipes, Annu. Rev. Fluid Mech. 15 (1) (1983) 461–512, https://doi.org/10.1146/annurev.fl.15.010183.002333.

[38] C.W. Oseen, Über die Stoke'sche Formel und über eine verwandte Aufgabe in der Hydrodynamik Arkiv Mat, Astron. och Fysik 6 (1910) 1.

[39] E.S. Asmolov, The inertial lift on a spherical particle in a plane Poiseuille flow at large channel Reynolds number, J. Fluid Mech. 381 (1999) 63–87, https://doi.org/10.1017/S0022112098003474.

[40] S. Razavi Bazaz, A. Mashhadian, A. Ehsani, S.C. Saha, T. Krüger, M. Ebrahimi Warkiani, Computational inertial microfluidics: a review, Lab Chip 20 (6) (2020) 1023–1048, https://doi.org/10.1039/C9LC01022J.

[41] D. Li, L. Song, C. Zhang, L. Yu, X. Xuan, A depth-averaged model for Newtonian fluid flows in shallow microchannels, Phys. Fluids 33 (1) (2021), 012002, https://doi.org/10.1063/5.0035167.
[42] J. Su, X. Chen, Y. Zhu, G. Hu, Machine learning assisted fast prediction of inertial lift in microchannels, Lab Chip 21 (13) (2021) 2544–2556, https://doi.org/10.1039/D1LC00225B.
[43] D. Di Carlo, D. Irimia, R.G. Tompkins, M. Toner, Continuous inertial focusing, ordering, and separation of particles in microchannels, Proc. Natl. Acad. Sci. USA 104 (48) (2007) 18892–18897, https://doi.org/10.1073/pnas.0704958104.
[44] R. Nasiri, A. Shamloo, S. Ahadian, L. Amirifar, J. Akbari, M.J. Goudie, K. Lee, N. Ashammakhi, M.R. Dokmeci, D. Di Carlo, A. Khademhosseini, Microfluidic-based approaches in targeted cell/particle separation based on physical properties: fundamentals and applications, Small 16 (29) (2020), 2000171, https://doi.org/10.1002/smll.202000171.
[45] Y.-J. Park, T. Yu, S.-J. Yim, D. You, D.-P. Kim, A 3D-printed flow distributor with uniform flow rate control for multi-stacked microfluidic systems, Lab Chip 18 (8) (2018) 1250–1258, https://doi.org/10.1039/C8LC00004B.
[46] M. Darekar, K.K. Singh, J.M. Joshi, S. Mukhopadhyay, K.T. Shenoy, Single-stage microscale solvent extraction in parallel microbore tubes using a monoblock distributor with integrated microfluidic junctions, Separ. Sci. Technol. 52 (14) (2017) 2213–2223, https://doi.org/10.1080/01496395.2017.1279181.
[47] S. Jespers, S. Deridder, G. Desmet, A microfluidic distributor combining minimal volume, minimal dispersion and minimal sensitivity to clogging, J. Chromatogr. A 1537 (2018) 75–82, https://doi.org/10.1016/j.chroma.2018.01.029.